

Research article

Zhao Chen^{a,*}, Sai Chen^a, Yangyang Wang and Lin Xiao^{*}

Tunable atom-trapping based on a plasmonic chiral metamaterial

<https://doi.org/10.1515/nanoph-2019-0163>

Received June 5, 2019; revised July 10, 2019; accepted July 11, 2019

Abstract: Chiral metamaterials provide a very convenient way to actively regulate the light field via external means, which is very important in nanophotonics. However, the very weak chiral response of a generally planar metamaterial severely limits its application. Therefore, it is important to design a system with large circular dichroism. Here we report an optical metamaterial with strong chirality in a bilayer gear-shaped plasmonic structure and consider this chiral response of such fields on tunable atom (⁸⁷Rb) trapping. Simulation results show that maximum chiral response is observed when the two layers of the gear-shaped structures are rotated from each other by an angle of 60° at $\lambda = 760$ nm. Also, we demonstrate an active tunable potential for three-dimensional stable atom-trapping with tunable range of position and potential of a neutral atom of ~ 58 nm and $\sim 1.3N$ mK (N denotes the input power with unit mW), respectively. In addition, the trap centers are about hundreds of nanometers away from the structure surface, which ensures the stability of the trapping system. The regulation of neutral atom trapping broadens the application of chiral metamaterials and has potential significance in the manipulation of cold atoms.

Keywords: surface plasmons; atom-trapping; chiral metamaterials.

1 Introduction

The configuration of metamaterials which can be designed and manipulated to obtain extraordinary properties has attracted considerable attention in recent years [1, 2]. A wide variety of functional devices can be realized in such systems [3], including but not limited to sensors [4, 5], polarizers [6–8], and photodetectors [9–12]. Among them, there is a class of metamaterials with a special structure, named chiral metamaterials, which shows different electromagnetic response, also called chirality, to right- and left-handed circularly polarized (RCP and LCP) light [13–15]. This unique optical response renders chiral metamaterials highly promising candidates for a variety of applications [16–30]. In general, chiral metamaterials are designed to be single-layered (planar chiral metamaterial) because of the relative ease of their fabrication [16–21]. However, the chiral responses are very weak and typically require oblique incidence. In order to obtain a large chiral response in the case of normal incidence, various novel chiral structures have been designed [31–34]. For instance, Cui et al. demonstrated a giant chiral optical response from a twisted-arc metamaterial [31]. Chen et al. realized strong optical chirality based on slanted plasmonic nanoapertures [32]. Rodrigus et al. proposed a double-layered ellipse hole to achieve intensity-dependent modulation [33]. Rajaei et al. experimentally reported giant circular dichroism (CD) with ramp-shaped plasmonic nanostructures [34]. In the above-mentioned works [16–34], we find that all designs are based on structure-surface-confined field effects to realize a variety of applications while ignoring spatial effects such as neutral atom trapping, an application that requires a noncontact field to be implemented.

As is known, optically trapped atoms, e.g. ⁸⁷Rb, ¹³³Cs, have been used for precision metrology and quantum information processing because a neutral atom is an excellent frequency reference and atoms trapped in an optical field have long coherence times and long lifetimes [35]. At present, a common method of trapping neutral atoms is by using optical dipole traps [36]. This kind of trapping uses the potential well generated by the incident field to push/pull the atom into the potential dip

^aZhao Chen and Sai Chen are co-first authors.

***Corresponding authors: Zhao Chen and Lin Xiao**, Nanophotonics and Optoelectronics Research Center, Qian Xuesen Laboratory of Space Technology, China Academy of Space Technology, Beijing 100094, China, e-mail: chenzhao@qxslab.cn (Z. Chen); xiaolin@qxslab.cn (L. Xiao). <https://orcid.org/0000-0002-3880-3664> (Z. Chen)

Sai Chen and Yangyang Wang: Nanophotonics and Optoelectronics Research Center, Qian Xuesen Laboratory of Space Technology, China Academy of Space Technology, Beijing 100094, China

and is independent of the particular sublevel state of the trapped atoms. Much of the work on atom trapping has been achieved using optical nanofibers [37–42]. However, the optical nanofiber cannot enhance the light field and requires a large input power, which will reduce the life of the trapped atoms. On the other hand, in order to increase the stability of the trapping system, the surface potential must be overcome, which increases the complexity of the system and difficulty of the experiment [37–42]. To address this problem, neutral atom trapping based on surface plasmon (SP) was proposed [43, 44], and later a plasmonic nanohole-array-based stable 3D atom trapping was also achieved [45]. Nevertheless, creating tunable optical traps compatible with optical nanostructures is still a challenge, so it is essential to make such trapping tunable via external means at the nanoscale.

In this article, we report a novel type of chiral metamaterial for atom-trapping based on plasmonic, bilayered, gear-shaped nanoapertures, with the layers rotated from each other by an angle of 60° in silver films. The basic design principle is to obtain the largest transmitted power difference between RCP and LCP at the blue detuned trap wavelength for ^{87}Rb . Simulation results show that the maximum differential transmittance is observed at $\lambda = 760 \text{ nm}$. Also, an active tunable potential for 3D stable optical trapping at the nanoscale is demonstrated. By

changing the phase of the circularly polarized light (RCP to LCP or LCP to RCP), the tunable range of position and potential of the trapped atoms is about $\sim 58 \text{ nm}$ and 1.3 N mK because of the different near-field scattering intensities. Our structure is very compact and easy to fabricate by the focused ion beam milling process. Combining neutral atom trapping with chiral metamaterial plasmonic structures would open the possibility of achieving ultracompact functional optical components in highly integrated optics.

2 Designed chiral plasmonic structure

The schematic diagram of our setup is illustrated in Figure 1A. The unit cell of the novel chiral plasmonic structure consists of two thin silver layers ($h = 90 \text{ nm}$) each of which has been perforated in the shape of a gear, and which are rotated from each other by an angle $\alpha = 60^\circ$. The point O in Figure 1A denotes the origin of coordinate, and the direction of the arrow is positive. The second film layer is grown on a silica (refractive index $n_{\text{silica}} = 1.45$) substrate and is separated from the first layer by a thin silica layer of $d = 350 \text{ nm}$. The silica layers are continuous without any hole in their structure, and the silica does not fill the chiral

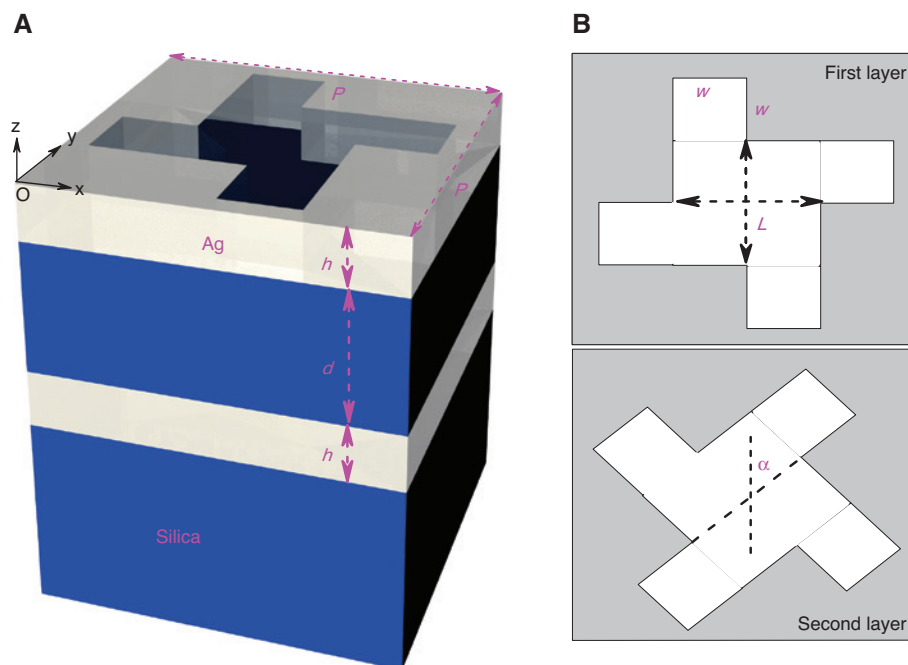


Figure 1: Schematic of chiral metamaterial.

(A) A single unit cell of the gear-shaped metamaterial array and the geometrical parameter symbols. (B) The top view of the silver film: the two layers of the gear-shaped structure are rotated from each other by an angle $\alpha = 60^\circ$.

opening at the bottom metal. Figure 1B shows the top view of the first and second silver films. The proposed structure can be made by plasma-enhanced chemical vapor deposition (PECVD) and focused-ion-beam (FIB) writing. The relative permittivity of silver is taken from the literature [46] and expanded using the method of interpolation by 1 nm. The module *Wave Optics* (Electromagnetic Waves, Frequency Domain) in COMSOL Multiphysics 5.2a is used to investigate the optical response of the proposed structure. Here, the periodic boundary conditions are set to the x - and y -direction of the unit cell, and perfectly matched layer absorbing conditions are set on the top (with Port 2 “off”)/bottom (with Port 1 “on”) sides. Then, the S -parameters of $abs(ewfd.S21)^2$, which can be extracted from the model, express the transmission spectrum of the system. The CP light port modes are set as the electric mode field: $E_x = \exp(-j \times k_0 \times n_{\text{silica}} \times z)$, $E_y = \exp(-j \times k_0 \times n_{\text{silica}} \times z + ja)$, and $E_z = 0$ ($k_0 = 2\pi/\lambda$ denotes free-space wave vector, $a \in (0, 2\pi)$ represents the phase of CP light, and $a = \pi/2$ or $3\pi/2$ corresponds to LCP or RCP, respectively). The other optimized parameters are set as follows: $P = 700$ nm, $L = 300$ nm, and $w = 150$ nm. The purpose of optimizing the parameters is to obtain the maximum chiral response at the trapping wavelength so as to adjust the position and potential energy of the trapped atoms to the maximum extent. The calculated transmission spectra for RCP (black curve) and LCP (red curve) incidences are shown in Figure 2A. It is clearly observed that a pronounced plasmonic resonance is present at $\lambda = 760$ nm under RCP incidence, whereas the transmission under LCP incidence is strongly suppressed, leading to a large differential transmittance. In order to distinguish it from circular dichroism (CD), a typical feature of a chiral response, which is defined as the

difference in absorption of RCP and LCP [13–15], we named the differential transmittance as CD_T, which is shown in Figure 2B. The maximum value in Figure 2B means that the difference in electric intensities between RCP and LCP is the largest, which provides a basis for subsequent adjustment of potential and position for trapped neutral atoms. Figure 2C,D displays the electric field intensity distributions (the positions of the first and second layer correspond to the plane $z=0$ and $z=-440$ nm for one unit cell, respectively.) under RCP and LCP illumination at the resonant wavelength $\lambda = 760$ nm. The distributions of the hot spots related to the enhancement of the electric field show a clear dependence on the polarization of the incident light, resulting in a large difference in transmittance of RCP and LCP light. Beyond that, the circular state of polarization is perfectly preserved in the transmitted wave, with a conversion ratio less than 0.16% between RCP and LCP, shown as the inset in Figure 2A. The appearance of the CD_T spectrum can be attributed to the broken mirror symmetry due to the index mismatch between the superstrate and the substrate [47].

3 Analysis of atom-trapping for ^{87}Rb

According to previous literature [44, 45, 48], we know that the near-field scattering effect of the periodic plasmonic structure can produce a local electric field minimum in the spatial extent of the system. In our system, RCP and LCP light incidence cause different scattering intensities, which in turn make the local electric field minimum adjustable. Here, we consider this phenomenon in neutral atom (^{87}Rb) trapping. To better understand the advantages

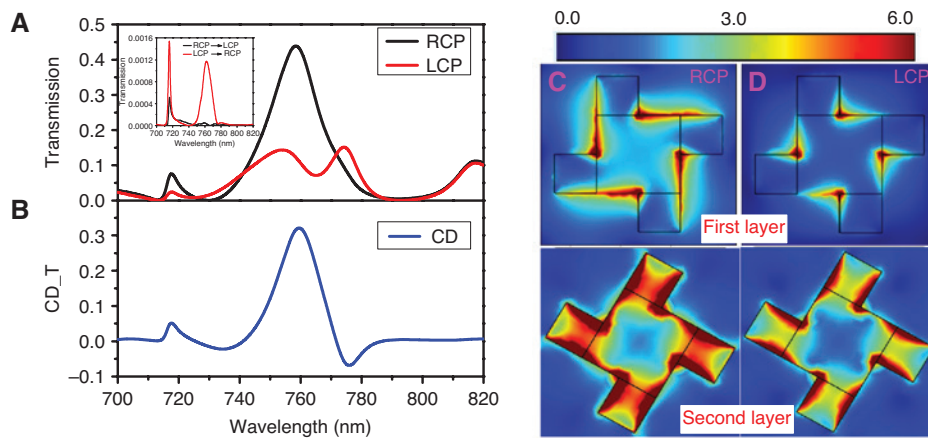


Figure 2: The circular dichroism of the structure.

(A) Simulation results of the normalized zero-order transmission spectrum for RCP (black curve) and LCP (red curve) incidences. (B) The CD_T spectrum corresponding to (A). Electric field intensity maps under (C) RCP and (D) LCP excitations at $\lambda = 760$ nm. Inset: simulated circular-polarization-conversion spectra.

of the system in terms of atom-trapping, we plot the spatial electric field intensity ($|E|^2$) distributions of the proposed structure at $\lambda=760$ nm at $x=0$ or $y=0$ plane for one unit cell, which are shown in Figure 3A,B for RCP and LCP excitations, respectively. (It is to be noted that the electric field distributions are the same at $x=0$ or $y=0$ plane only when LCP or LCP light excites because of the peculiarity of the structure.) The resonant wavelength $\lambda=760$ nm is selected to be blue-detuned to the D_2 line of ^{87}Rb atoms [45, 48]. By the way, the proposed trapping platform is suitable for trapping neutral atoms with all the transition wavelengths greater than 760 nm, e.g. ^{133}Cs . Apparently, a trap center (local electric field minimum) emerges at each plot, which is about hundreds of nanometers away from the structure surface. Here, ds ($ds=379$ nm for LCP and $ds=321$ nm for RCP) denotes the distance between the structure surface ($z=0$) and the trap center. A neutral atom, i.e. ^{87}Rb atom, can be trapped in the trap center via optical dipole forces with blue-detuned light [36].

As is known, a neutral atom in an electric field will be affected by two kinds of potentials [36]. One is the optical dipole potential, U_{opt} , which can be expressed as $U_{\text{opt}} = -\frac{1}{4}\alpha|E|^2$. Here, α is the reduced polarizability and its expression is taken from [49]. We considered eight transition wavelengths of ^{87}Rb , and the calculated value is $\alpha \approx -7.87 \times 10^{-38}$ F \cdot m 2 at the trapping wavelength $\lambda=760$ nm. Therefore, according to the electric field intensity distribution, we can easily get the optical dipole potential of the trapped atom. The other is the surface potential U_{sur} , which can play an important role in the trapping characteristics when the atom is close to the structure surface (less than 100 nm) [50]. Notably, in our system the newly emerged trap center is about hundreds of nanometers (321 nm for RCP and 379 nm for LCP)

away from the structure surface, so U_{sur} can be negligible relative to U_{opt} in our calculations. This is why our trapping system is very stable. Thus, in this article, we use U_{opt} as the total potential of the trapped atom. For quantitative description of the trapping properties, we calculate U_{opt} along the pink dashed line in Figure 3A,B, shown in Figure 3C with input power $P_0=1$ mW. Here, $\Delta s=58$ nm denotes the movable range of the trapped atom during RCP and LCP conversion. Namely, we can tune the position of the trapped atoms by only changing the phase difference a . The absolute value $|U_{\text{eff-RCP}} - U_{\text{eff-LCP}}|$ is the potential tunable factor, and for input power $P_0=N$ mW, the tunable nanopotential is $\Delta_{\text{trap}} = N \times |U_{\text{eff-RCP}} - U_{\text{eff-LCP}}| = 1.3N$ mK. Figure 3D quantitatively shows the position of the trapped atom at any phase difference a within one phase cycle. Here, the phase difference $a \in (0, 2\pi/40, 2\pi)$, therefore, $a(1)$ denotes LCP (B) and $a(31)$ stands for RCP (D). It is clear that the maximum range of movement of the trapped atom is $\Delta s=58$ nm (B \rightarrow D or D \rightarrow B). Although the trapped atom has the same position at points A and C, the potential is different in the same plane because of the fourfold rotation symmetry only of the structure. In order to visually observe the movement of the trapped atoms, the animation graphics of the trap centers is displayed in Supporting Information. It can be clearly observed that the trap centers are moving back and forth with the change in a . In addition, we can find that the field distributions at $a(1)$ (point A) and $a(21)$ (point C) are obviously different. Compared to our previous work [48], the proposed structure is relatively compact, the CD_T response is larger, and one single unit cell can realize all the features. Although the movable range of the trapped atom is similar, the tunable potential is increased by about 2.6 times, which greatly increases the practicability of the system.

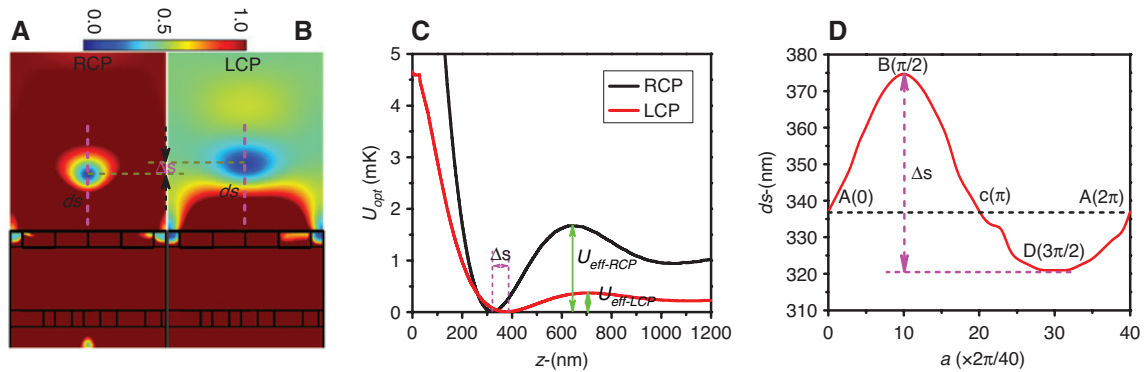


Figure 3: Quantitative description for the trapping ability of the system.

Normalized spatial electric field intensity ($|E|^2$) distributions for (A) RCP and (B) LCP excitations at $x=0$ or $y=0$ plane. (C) Corresponding optical dipole potential U_{opt} distributions along the pink dashed lines in A and B with input power $P_0=1$ mW. (D) The variation law of ds with change in a .

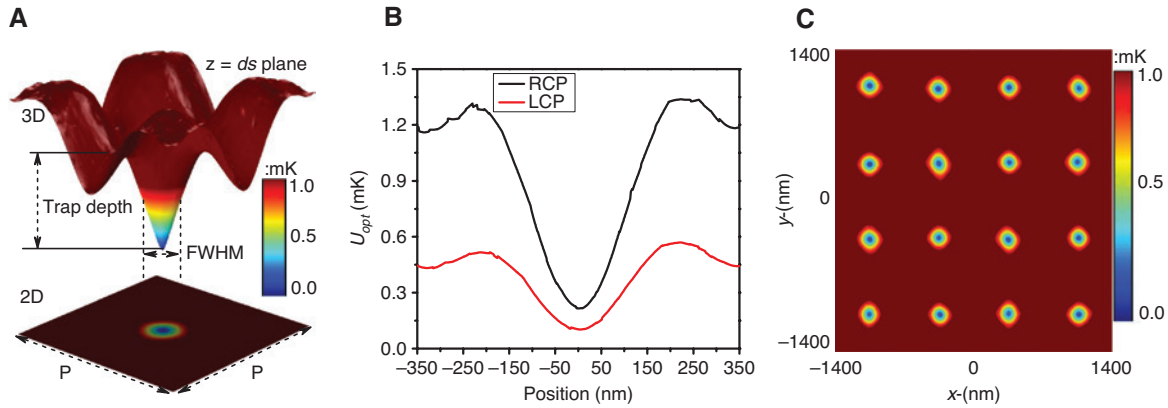


Figure 4: 3D trapping property of the system.

(A) Distributions of U_{opt} of the $z = ds$ plane in 2D and 3D at the trapping wavelength $\lambda = 760$ nm for one unit cell. (B) Corresponding optical dipole potential U_{opt} distributions for RCP (black line) and LCP (red line) through x/y centering direction. (C) Periodic arrays at $z = ds$ in the $x-y$ plane.

In order to further analyze the 3D trapping property of the system, we plot the distributions of U_{opt} in the $x-y$ plane at the trapping wavelength $\lambda = 760$ nm, as shown in Figure 4A. Figure 4B shows the corresponding optical dipole potential (U_{opt}) distributions for RCP (black line) and LCP (red line) through the x or y centering direction. It can be easily seen that the trap depths are about 1.1 mK and 0.42 mK for RCP and LCP incidences, respectively, with input power $P_0 = 1$ mW. The full width at the half-maxima (FWHMs) are both about 225 nm for RCP and LCP, which can be used to confine and trap a single atom [49]. Manipulation of a single atom can be used to verify basic physical laws and for accurate measurements of physical constants. Figure 4C shows the trap centers of periodic arrays at $z = ds$ in the $x-y$ plane. (Here, we use 4×4 unit cells to represent an infinitely extended array. However, due to limitations of computer memory and because the Comsol Multiphysics software mesh cannot be evenly divided, the trap centers show a small asymmetry.) The periodic structure guarantees the uniformity of trap depths in each unit cell, which greatly reduces the detection error due to the variance of cooling efficiency and the photon scattering rate from each atom [38–42, 45, 48]. In addition, atom array trapping can be used to realize resonance fluorescence. Through the above analysis, a tunable, stable 3D atom array trapping independent of the surface potential based on a plasmonic chiral metamaterial is demonstrated. The ability to regulate neutral atoms at the subwavelength scale would enable quantum network capabilities and large-scale quantum communications. In addition, our systems can also enable refractive index sensors, as well as circular polarization detectors, which are very important in nanophotonics.

4 Conclusion

In conclusion, we have demonstrated tunable and stable 3D atom array trapping based on the large circular dichroism in a plasmonic chiral metamaterial made up of a double-layer gear-shaped structure. Simulation results showed that under RCP excitation, there is a transmission resonance peak at $\lambda = 760$ nm, while the transmission is almost completely suppressed by LCP excitation. Because of the near-field scattering, a trap center, about hundreds of nanometers (321 nm for RCP and 379 nm for LCP) away from the structure surface, emerges, which guarantees the stability of the trapped atoms. Different electric field intensities make the trapped atoms tunable by altering the phase of the CP light. The proposed structure can be easily fabricated and integrated on a chip. This type of atom-trapping method, based on the regulation of LCP and RCP light, holds promise for atomic on-chip integration, which will have great significance in quantum information processing and nanophotonics.

Acknowledgments: This work was supported by the National Natural Science Foundation of China (NSFC) (11704013), Funder Id: <http://dx.doi.org/10.13039/501100001809> and the National Science and Technology Innovation Special Zone Program of China.

References

- [1] Engheta N, Ziolkowski RW, editors. *Metamaterials: physics and engineering explorations*. John Wiley & Sons, 2006.
- [2] Cui TJ, Smith DR, Liu R. *Metamaterials*. New York, NY, Springer, 2010.

- [3] Tong XC. *Functional metamaterials and metadevices*. Bolingbrook, IL, Springer, 2018.
- [4] He Y, Lawrence K, Ingram W, Zhao Y. Circular dichroism based refractive index sensing using chiral metamaterials. *Chem Commun* 2016;52:2047–50.
- [5] Wang W, Yan F, Tan S, Zhou H, Hou Y. Ultrasensitive terahertz metamaterial sensor based on vertical split ring resonators. *Photon Res* 2017;5:571–7.
- [6] Zhao Y, Alu A. Manipulating light polarization with ultrathin plasmonic metasurfaces. *Phys Rev B* 2011;84:205428.
- [7] Zhao Y, Belkin M, Alu A. Twisted optical metamaterials for planarized ultrathin broadband circular polarizers. *Nat Commun* 2012;3:870.
- [8] Ji R, Wang S, Liu X, Chen X, Li W. Broadband circular polarizers constructed using helix-like chiral metamaterials. *Nanoscale* 2016;8:14725–9.
- [9] Song S, Ma X, Pu M, et al. Tailoring active color rendering and multiband photodetection in a vanadium-dioxide-based metamaterial absorber. *Photon Res* 2018;6:492–7.
- [10] Venuthurumilli PK, Ye PD, Xu X. Plasmonic resonance enhanced polarization sensitive photodetection by black phosphorus in near infrared. *ACS Nano* 2018;12:4861–7.
- [11] Bai Q. Manifestation of the spontaneous parity-time symmetry breaking phase transition in hot-electron photodetection based on a tri-layered metamaterial. *Nanophotonics* 2019;8:495–504.
- [12] Lee H, Lee H, Park JY. Direct imaging of surface plasmon-driven hot electron flux on the Au nanoprism/TiO₂. *Nano Lett* 2019;19:891–6.
- [13] Schäferling M. *Chiral nanophotonics*. Cham, Switzerland, Springer International Publishing, 2017.
- [14] Qu Y, Huang L, Wan L, Zhang Z. Giant circular dichroism induced by tunable resonance in twisted Z-shaped nanostructure. *Opt Express* 2017;15:5480–7.
- [15] Wang Z, Wang Y, Adamo G, Teng J, Sun H. Induced optical chirality and circularly polarized emission from achiral CdSe/ZnS quantum dots via resonantly coupling with plasmonic chiral metasurfaces. *Laser Photon Rev* 2019;13:1800276.
- [16] Klimov VV, Zabkov IV, Pavlov AA, Shiu RC, Chan HC, Guo GY. Manipulation of polarization and spatial properties of light beams with chiral metafilms. *Opt Express* 2016;24:6172–85.
- [17] Ye W, Yuan X, Guo C, Zhang J, Yang B, Zhang S. Large chiroptical effects in planar chiral metamaterials. *Phys Rev App* 2017;7:054003.
- [18] Feng X, Bai Y, Jing Z, et al. Enhanced circular dichroism of tilted zigzag-shaped nanohole arrays. *Appl Opt* 2019;58:177–81.
- [19] Dyakov SA, Semenenko VA, Gippius NA, Tikhodeev SG. Magnetic field free circularly polarized thermal emission from a chiral metasurface. *Phys Rev B* 2018;98:235416.
- [20] Qi J, Zhang M, Zhang Y, et al. Multiband circular dichroism from bilayer rotational F4 nanostructure arrays. *Appl Opt* 2019;58:479–84.
- [21] Bai Y, Wang T, Ullah H, Qu Y, Abudukelimu A, Zhang Z. Asymmetric transmission in the planar chiral nanostructure induced by electric and magnetic resonance at the same wavelength. *Annalen der Physik* 2019;531:1800469.
- [22] Saklari I, Yin X, Nesterov ML, Terzaki K, Xomalis A, Farsari M. 3D chiral plasmonic metamaterials fabricated by direct laser writing: the twisted omega particle. *Adv Opt Mater* 2017;5:1700200.
- [23] Pan M, Li Q, Hong Y, Cai L, Lu J, Qiu M. Circular-polarization-sensitive absorption in refractory metamaterials composed of molybdenum zigzag arrays. *Opt Express* 2018;26:17772–80.
- [24] Liang S, Zhang W, Yuan J, et al. In-plane gap plasmon induced strong circular dichroism in double-layer Archimedean planar metamaterials. *Opt Mater Express* 2018;8:2870–9.
- [25] Wu Z, Chen X, Wang M, Dong J, Zheng Y. High-performance ultrathin active chiral metamaterials. *ACS Nano* 2018;12:5030–41.
- [26] Wang Z, Ai B, Zhou Z, Guan Y, Mohwald H, Zhang G. Free-standing plasmonic chiral metamaterials with 3D resonance cavities. *ACS Nano* 2018;12:10914–23.
- [27] Chen Y, Gao J, Yang X. Direction-controlled bifunctional metasurface polarizers. *Laser Photon Rev* 2018;12:1800198.
- [28] Yang S, Liu Z, Hu S, et al. Spin-selective transmission in chiral folded metasurfaces. *Nano Lett* 2019. DOI: 10.1021/acs.nanolett.8b04521.
- [29] Klos G, Miola M, Sutherland DS. Increased refractive index sensitivity by circular dichroism sensing through reduced substrate effect. *J Phys Chem C* 2019;123:7347–55.
- [30] Cao T, Mao L, Qiu Y, et al. Fano resonance in asymmetric plasmonic nanostructure: separation of sub-10 nm enantiomers. *Adv Opt Mater* 2019;7:1801172.
- [31] Cui Y, Kang L, Lan S, Rodriues S, Cai W. Giant chiral optical response from a twisted-arc metamaterial. *Nano Lett* 2014;14:1021–5.
- [32] Chen Y, Gao J, Yang X. Chiral metamaterials of plasmonic slanted nanoapertures with symmetry breaking. *Nano Lett* 2018;18:520–7.
- [33] Rodrigus SP, Lan S, Kang L, et al. Intensity-dependent modulation of optically active signals in a chiral metamaterial. *Nat Commun* 2017;8:10462.
- [34] Rajaei M, Zeng J, Albooyeh M, et al. Giant circular dichroism at visible frequencies enabled by plasmonic pamp-shaped nanostructures. *ACS Photon* 2019;6:924–31.
- [35] Lee J, Park DH, Mittal S, Dagenais M, Rolston SL. Integrated optical dipole trap for cold neutral atoms with an optical waveguide coupler. *New J Phys* 2013;15:043010.
- [36] Grimm R, Weidemuller M. Optical dipole traps for neutral atoms. *Adv At Mol Opt Phys* 2000;42:1–39.
- [37] Nieddu T, Gokhroo V, Chormaic SN. Optical nanofibers and neutral atoms. *J Opt* 2016;18:053001.
- [38] Qi X, Baragiola BQ, Jessen PS, Deutsch IH. Dispersive response of atoms trapped near the surface of an optical nanofiber with applications to quantum nondemolition measurement and spin squeezing. *Phys Rev A* 2016;93:023817.
- [39] Goban A, Choi KS, Alton DJ, et al. Demonstration of a state-insensitive, compensated nanofiber trap. *Phys Rev Lett* 2012;109:033603.
- [40] Vetsch E, Reitz D, Sague G, Schmidt R, Dawkins ST, Rauschenbeutel A. Optical interface created by laser-cooled atoms trapped in the evanescent field surrounding an optical nanofiber. *Phys Rev Lett* 2010;104:203603.
- [41] Balykin VI, Hakuta K, Le Kien F, Liang JQ, Morinaga M. Atom trapping and guiding with a subwavelength-diameter optical fiber. *Phys Rev A* 2004;70:011401(R).
- [42] Le Kien F, Balykin VI, Hakuta K. Atom trap and waveguide using a two-color evanescent light field around a subwavelength-diameter optical fiber. *Phys Rev A* 2004;70:063403.

- [43] Chang DE, Thompsin JD, Park H, et al. Trapping and manipulation of isolated atoms using nanoscale plasmonic structures. *Phys Rev Lett* 2009;103:123004.
- [44] Gullans M, Tiecke T, Chang DE, et al. Nanoplasmonic lattices for ultracold atoms. *Phys Rev Lett* 2012;109:235309.
- [45] Chen Z, Zhang F, Zhang Q, et al. Blue-detuned optical atom trapping in a compact plasmonic structure. *Photon Res* 2017;5:436–40.
- [46] Johnson PB, Christy RW. Optical constants of the noble metals. *Phys Rev B* 1972;6:4370–9.
- [47] Kuwata-Gonokami M, Saito N, Ino Y, et al. Giant optical activity in quasi-two-dimensional planar nanostructures. *Phys Rev Lett* 2005;95:227401.
- [48] Chen Z, Zhang F, Duan X, Zhang T, Gong Q, Gu Y. Chiral-plasmon-tuned potentials for atom trapping at the nanoscale. *Adv Opt Mater* 2018;6:1800261.
- [49] Zhang PF, Li G, Zhang TC. Subwavelength optical dipole trap for neutral atoms using a microcapillary tube tip. *J Phys B: At Mol Opt Phys* 2017;50:045005.
- [50] Chang DE, Sinha K, Taylor JM, Kimble HJ. Trapping atoms using nanoscale quantum vacuum forces. *Nat Commun* 2014;5:4343.

Supplementary Material: The online version of this article offers supplementary material (<https://doi.org/10.1515/nanoph-2019-0163>).